Computers in Biology and Medicine 186 (2025) 109668

Contents lists available at ScienceDirect

Computers in Biology and Medicine

journal homepage: www.elsevier.com/locate/compbiomed

Quantifying the influence of combined lung and kidney support using a cardiovascular model and sensitivity analysis-informed parameter identification

Jan-Niklas Thiel [a,*], Ana Martins Costa [b], Bettina Wiegmann [c,d,e], Jutta Arens [b], Ulrich Steinseifer [a], Michael Neidlin [a]

[a] Department of Cardiovascular Engineering, Institute of Applied Medical Engineering, Medical Faculty, RWTH Aachen University, Forckenbeckstraße 55, 52074, Aachen, Germany
[b] Engineering Organ Support Technologies group, Department of Biomechanical Engineering, University of Twente, Drienerlolaan 5, 7522, NB, Enschede, the Netherlands
[c] Department for Cardiothoracic, Transplantation and Vascular Surgery, Hannover Medical School, Carl-Neuberg-Straße 1, 30625, Hannover, Germany
[d] Implant Research and Development (NIFE), Lower Saxony Center for Biomedical Engineering, Stadtfelddamm 34, 30625, Hannover, Germany
[e] German Center for Lung Research (DZL), Carl-Neuberg-Straße 1, 30625, Hannover, Germany

ARTICLE INFO

Keywords:
Lumped parameter modeling
Cardiovascular modeling
Global sensitivity analysis
Parameter identification
Extracorporeal membrane oxygenation
ECMO
Continuous renal replacement therapy

ABSTRACT

The combination of extracorporeal membrane oxygenation (ECMO) and continuous renal replacement therapy (CRRT) pose complex hemodynamic challenges in intensive care. In this study, a comprehensive lumped parameter model (LPM) is developed to simulate the cardiovascular system, incorporating ECMO and CRRT circuit dynamics. A parameter identification framework based on global sensitivity analysis (GSA) and multi-start gradient-based optimization was developed and tested on 30 clinical data points from eight veno-arterial ECMO patients. To demonstrate feasibility, the model is used to analyze nine CRRT-ECMO connection schemes under varying flow conditions for a single patient.

Our results indicate that CRRT has a notable impact on the cardiovascular system, with changes in pulmonary artery pressure of up to 203 %, highly dependent on ECMO flow. The GSA enabled the systematic and agnostic identification of a subset of model parameters used in the calibration process. The established parameter estimation framework is fast and robust, as no manual tuning of algorithm parameters is required, and achieves high correlations between simulation and experimental data with $R^2 > 0.98$. It uses modeling methods that could pave the way for real-time applications in intensive care.

This open-source framework provides a valuable tool for the systematic evaluation of combined ECMO and CRRT, which can be used to develop standardized treatment protocols and improve patient outcomes in critical care. This model provides a good basis for addressing research questions related to mechanical circulatory and respiratory support and presents tools to help move towards a digital twin in healthcare.

1. Introduction

Extracorporeal membrane oxygenation (ECMO) is frequently used in intensive care medicine to treat cardiac and/or respiratory failure. It is used to partially or fully support heart/lung function in the sense of a "bridge to transplantation" or "bridge to recovery" [1]. An ECMO circuit consists of a pump, an oxygenator, and cannulae to drain and return oxygenated and decarboxylated blood. However, up to 70 % of patients develop an acute kidney injury during ECMO which can be attributed to the so-called lung-kidney crosstalk and the often reported fluid overload [2–5]. Additional continuous renal replacement therapy (CRRT) is therefore essential, but is also associated with higher morbidity and mortality [6–9].

The combined support of the lungs and kidneys can be realized in an integrated or separate manner. The separate approach requires a separate vascular access for each device [7,10–12]. This leads to a higher level of circuit complexity with an increased technical workload [13] and a significantly larger artificial surface area, as well as circulatory complications such as bleeding [14], thrombus formation, and infection [15], resulting in significantly higher healthcare costs [16,17]. In the

* Corresponding author. Institute of Applied Medical Engineering, Forckenbeckstraße 55, 52074, Aachen, Germany.
E-mail address: thiel@ame.rwth-aachen.de (J.-N. Thiel).

https://doi.org/10.1016/j.compbiomed.2025.109668
Received 11 July 2024; Received in revised form 11 December 2024; Accepted 7 January 2025
Available online 17 January 2025

integrated approach, CRRT is connected directly to the ECMO circuit. This presents challenges in controlling circuit pressure, which can lead to treatment interruptions, air entrapment, flow interruptions, and hemolysis [18,19]. This combined therapy still lacks a gold standard and its connection configuration varies depending on the operator's practice and proficiency. In total, there are nine different possibilities for connecting the CRRT circuit to the ECMO circuit (depicted in Fig. 2), which, together with the different cannula sizes, result in a wide variety of combinations.

In the context of the integrated approach, Wang et al. investigated the effect of different CRRT connection schemes on the pressures in the access and return lines of the CRRT circuit [20]. In-vitro experiments comparing six commonly used schemes showed significant pressure differences. In addition, a retrospective analysis of ten patients (seven veno-arterial ECMO (V-A ECMO), three veno-venous ECMO (V-V ECMO)) showed that changing the connection scheme can significantly reduce both access and return pressures. Wu et al. conducted a retrospective study with 100 patients who received a combined ECMO and CRRT therapy [21]. The patients were divided into groups receiving separate and integrated support. The results showed that the separate group had a significantly longer CRRT initiation time and a shorter filter lifetime. In addition, local bleeding was observed in approximately 90 % of patients in the separate group. While both studies highlight the advantages of the integrated approach for connecting CRRT to ECMO, the literature still lacks a systematic comparison of commonly used connection schemes under realistic patient conditions.

Lumped parameter models (LPM) offer a simplified approach to modeling the human cardiovascular system and the analysis of ECMO hemodynamics. These models, analogous to electrical circuits, use ordinary differential equations (ODE) based on the conservation of mass and momentum [22]. Various LPMs exist, with the most prominent ones being those developed by Arts et al. and Shi et al., which address different aspects of cardiovascular dynamics [23,24]. While models by Broomé et al. and Joyce et al. have investigated ECMO therapy, they have neglected to consider the dynamics of the ECMO circuit. Instead, they have focused on factors such as recirculation and gas exchange [25–31]. More sophisticated models, such as those developed by Fresiello et al. and Lazzari et al., integrate pump and cannula dynamics and serve as training tools, with a particular focus on usability through a graphical user interface rather than on the performance of the code [32,33]. The majority of the models presented are not open-source or lack automated and robust parameter identification, which limits their usability for other research questions and their application in clinical decision support. The latter requires models that are based on patient-specific data and support real-time recalibration without the need for extensive user interaction or in-depth user knowledge, in line with the concept of digital twins defined by Viceconti et al. [34]. To date, there is no such model that includes both ECMO and CRRT therapy.

In contrast, numerous studies have addressed the topic of parameter identification for more general cardiovascular models. Local optimization algorithms, such as trust-region-reflective methods [35,36] or Levenberg-Marquardt algorithms [37], are commonly used, but are highly dependent on the selected initial parameter values. In this context, the use of multi-start algorithms can provide guidance in finding a global optimum. The computation of gradients, which is typically performed by numerical differentiation, can result in inaccurate parameter estimation and numerical instability. Furthermore, this approach is known to be computationally expensive [38]. Automatic differentiation (AD) offers a faster and more stable alternative [38–42]. Global optimization techniques, such as the genetic algorithm, can also be utilized to identify a global optimum [43]. More sophisticated techniques, such as the unscented Kalman filter, can continuously update parameters in response to new measurements and are robust for dynamic, nonlinear systems [41,44–47].

As cardiovascular models often consist of a high number of parameters, estimating their parameters often suffers from parameter identifiability and high computational cost. In this regard, the selection of parameter subsets by ranking the influence of parameters by using global sensitivity analysis (GSA) and quantifying their independence of the effect on model outputs, also called parameter orthogonality, has been demonstrated to enhance the robustness and accuracy of parameter estimation [36–39,41,42,48,49].

Taken together, the combination of CRRT and ECMO therapy presents unanswered questions regarding optimal connection schemes and their impact on hemodynamics. LPMs appear to be a powerful tool for analyzing this problem, as they can provide measurements that are otherwise not available or very difficult to obtain in clinical practice. However, challenges remain in achieving robust and systematic parameter identification. Overcoming these challenges is essential to improve the accuracy and applicability of these models in clinical decision support.

The aim of this study is to develop a cardiovascular model that includes both the detailed ECMO and CRRT system and allows an arbitrary connection of both systems. A framework for fast parameter identification based on multi-start gradient-based optimization will be linked to this model, which will be benchmarked on a number of V-A ECMO patients. Parameter selection will be based on Sobol indices from a GSA. To demonstrate the feasibility of this modeling framework, a comprehensive analysis of combined ECMO and CRRT therapy will be performed for a single patient by investigating the impact of different CRRT connection schemes on patient and circuit dynamics at different ECMO flows.

2. Materials and methods

2.1. Patient data

The clinical data set includes eight patients (five male, aged 36–61 years; three female, aged 32–76 years) treated with V-A ECMO, each with up to four measurements, resulting in a total of 30 data points. It includes 13 data points from male and 17 from female patients. These patients suffered from cardiogenic shock, cardiomyopathy, or received a heart or lung transplant. The measured hemodynamic parameters, along with their respective median, minimum and maximum values, are presented in Table 1. The data set covers a wide range of clinically relevant operating points of ECMO therapy, including pump flows between 1 and 4 L/min. It comprises patients with both hypotension (MAP $<$65 mmHg) and hypertension (MAP $>$92 mmHg), as well as patients with a normal MAP.

2.2. Cardiovascular model

The model is inspired by the work of Shi et al. [24] and consists of the heart, systemic and pulmonary circulation, as shown in Fig. 1. The heart is modeled as four chambers with variable elasticity. The

Table 1
Measured hemodynamic parameters for 30 data points from eight V-A ECMO patients.

Parameter	Median	(Min, Max)
Systolic pressure (SP)	111.0	(70.0 , 183.0) mmHg
Diastolic pressure (DP)	69.5	(42.0 , 88.0) mmHg
Mean arterial pressure (MAP)	79.0	(55.0 , 113.0) mmHg
Mean pulmonary artery pressure (MPAP)	19.5	(6.0 , 30.0) mmHg
Pulmonary capillary wedge pressure (PCWP)	11.0	(7.0 , 15.0) mmHg
Cardiac output (CO)	3.4	(1.5 , 7.5) L/min
Pump flow (PF)	2.5	(1.2 , 3.8) mmHg

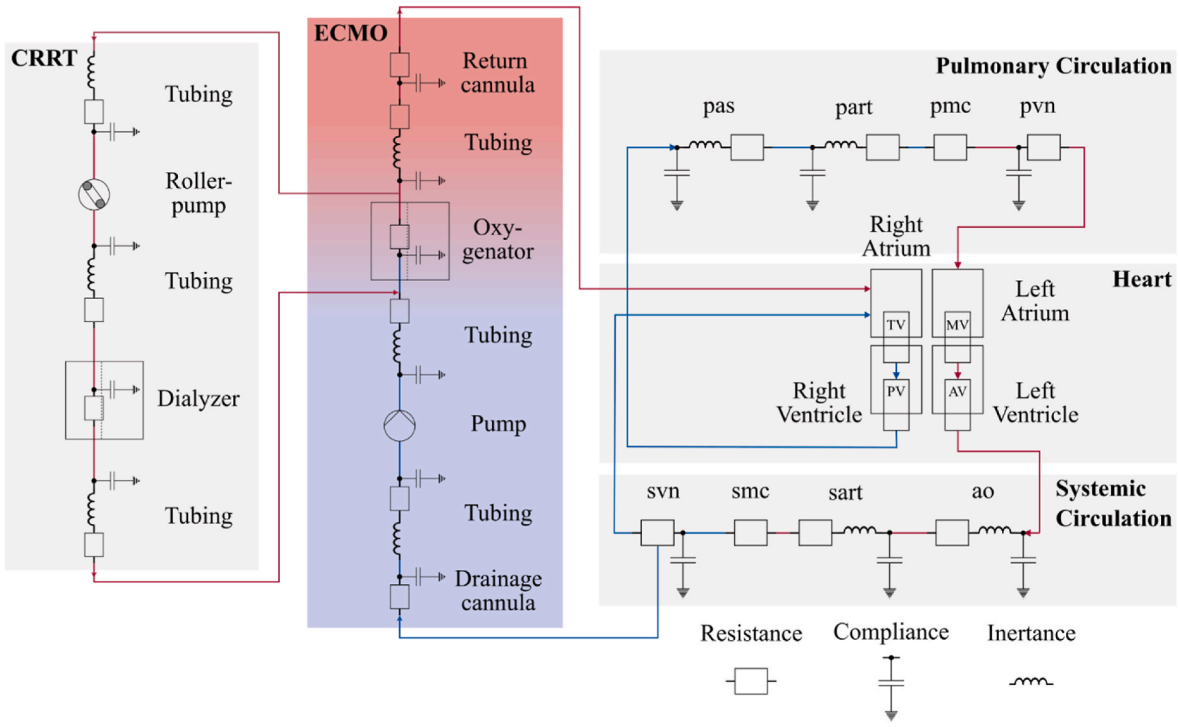

Fig. 1. Overview of the lumped parameter model. Cardiovascular system inspired by Shi et al. [24].

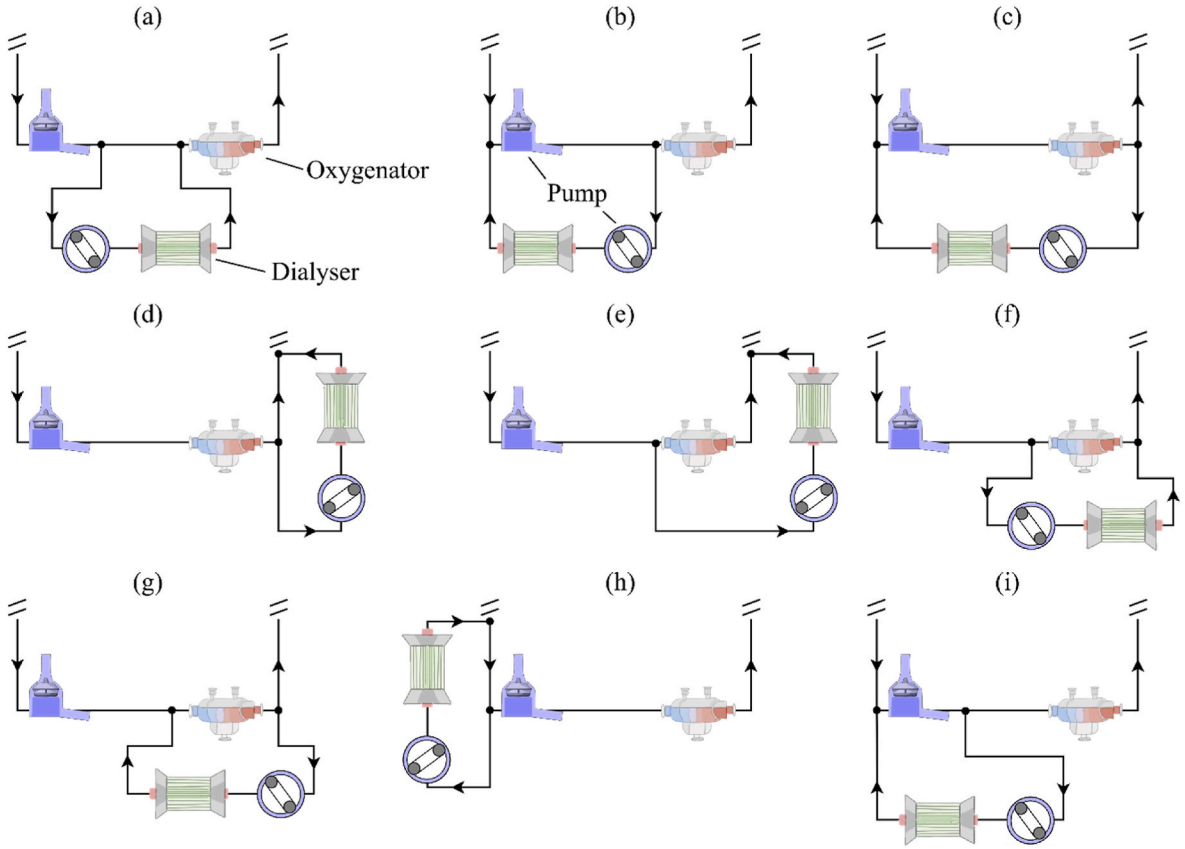

Fig. 2. Variations of CRRT connections to the ECMO circuit in CRRT-flow direction: a) post pump – pre oxygenator (pre oxy), b) pre oxy – pre pump, c) post oxy – pre pump, d) post oxy – pre return cannula (pre RC), e) pre oxy – pre RC, f) pre oxy – post oxy, g) post oxy – pre oxy, h) pre pump – post drainage cannula (post DC), i) post pump – pre pump. Of note: position of tubing e.g. between pump and oxygenator (compare (b) and (i)) is also taken into account by making a distinction between post pump and pre oxy.

piecewise-defined cosine activation function and elastance function for the atria are based on the model developed by Shi et al. [24]. These formulations contain the systolic and diastolic elastance of the left (Emaxla, Edla) and right atrium (Emaxra, Edra). For the ventricles, the elastance function was extended by an additional nonlinear term to account for a nonlinear diastolic elastance, which captures the effects of diastolic stretching of the ventricular wall [50], see equation (1):

$$p_j = V_j * e_v * Emax_j + (1 - e_v) * \left(\alpha_j * e^{\kappa_j * V_j} + \beta_j\right), with\ j = LV\ or\ RV \quad (1)$$

The relationship between the ventricular pressure p_j and volume V_j is described by the activation function e_v from Shi et al. [24], the systolic elastance $Emax_j$ of the respective ventricle, as well as the parameters α_j and β_j, representing the intercept and asymptotic pressure, and the stiffness coefficient κ_j. The heart valves, namely the tricuspid (TV), pulmonary (PV), mitral (MV), and aortic (AV) valves, have a diodic pressure drop quadratically dependent on the flow to control the direction of blood flow. Both the systemic and pulmonary circulation are divided into aortic sinus, artery, arteriole, capillary, and venous segments. Large vessels such as the aortic sinus and artery are highly elastic, and their flow is inherently pulsatile. Therefore, they are modeled with resistance, compliance, and inertance (RCL) elements, where resistance R accounts for frictional losses, compliance C for elasticity, and inertance L for blood inertia. Smaller arterioles and capillaries are mainly dominated by resistance effects, while veins have the function of collecting and storing blood and therefore also have compliance effects. The compartments of the cardiovascular system are abbreviated as follows: pas: pulmonary aortic sinus, part: pulmonary artery, pmc: pulmonary microcirculation, pvn: pulmonary vein, ao: aorta, sart: systemic artery, smc: systemic microcirculation, svn: systemic vein.

In our model, circuits for mechanical circulatory support such as ECMO and left ventricular assist devices (LVAD) can be connected to any compartment of the patient's cardiovascular system, allowing different V-A and V-V ECMO configurations and different modes of LVAD support to be studied. Additionally, the model allows CRRT to be connected to the ECMO circuit in many different configurations. ECMO cannulas are modeled using a resistance based on data sheets of established Getinge products while taking compliance effects into account. The tubes are modeled with RCL elements similar to Lazzari et al. [33] and Fresiello et al. [32] and their resistance is approximated by the Hagen-Poiseuille law assuming a laminar flow regime.

The ECMO pump is implemented using the analytical equations for rotary blood pumps (RBP) by Boes et al. [51], see equation (2):

$$H = an^2 - R_1 nQ - R_2 Q^2 - L\frac{dQ}{dt} + \begin{cases} 0, & Q > q_{inf} \\ R_{rec}\left(Q - q_{inf}\right)^2, & Q \le q_{inf} \end{cases} \quad (2)$$

This equation describes the relationship between pump head H and flow Q at a given pump speed n. In this model, the constants a, R_1, and R_2 represent terms that account for the pressure head, which includes both friction and incidence losses in the pump. The parameter L is the fluid inertia, which captures dynamic changes in pressure head. The term R_{rec} models part-load recirculation within the blade channels, with the inflection flow rate q_{inf} being a specific threshold for each pump, at which the slope of the H-Q curve changes. Given this implementation, theoretically any RBP can be integrated into the LPM without having to change anything in the code. For this study, the parameters of this equation were adapted to the two blood pumps Rotaflow RF-32 (Getinge/Maquet Cardiopulmonary GmbH, Germany) and DP3 (Fresenius Medical Care AG, Germany). The roller pumps are modeled by specifying a constant flow rate. The oxygenator and dialysis filter were modeled as RC elements, and their parameters were derived from the data sheets for Quadrox-i Adult and Small Adult (Getinge/Maquet Cardiopulmonary GmbH, Germany), Nautilus MC3 (MC3 Cardiopulmonary, USA) and Prismaflex M180 (Baxter International Inc., USA). This was done under the assumption of a linear relationship between pressure drop and flow.

The model compartments were initialized with physiological pressures representative of a healthy patient and a flow of zero. The model was implemented in *Python* using *JAX* with the possibility of just-in-time compilation and automatic differentiation. Therefore, all implemented functions are smooth, either inherently or by using techniques such as a smoothed Heaviside function. This ensures that the model is fully differentiable. The ODE system was solved using an 8th-order Runge-Kutta method, known as the Dormand Prince algorithm, which is implemented in the *Diffrax* package. An adaptive time step sizing approach was employed, with an initial time step size of 0.0005 s. The simulation time was set to 50 s to achieve cycle convergence. Only the last two cycles were evaluated.

We provide the full *Python* code with all described modules and parameter values at the GitHub link https://github.com/nikithiel/ECLIPSE. All parameter values and abbreviations used can also be found in Tables S-1, S-2, S-3, S-4 and S-5 in the Appendix.

2.3. Global sensitivity analysis

The influence of the model parameters on the model outputs and their interactions between each other were quantified using the Sobol method [52], which is implemented in the *SALib* package. Such variance-based Global sensitivity analysis aims to quantify the effect of variances in the input parameters on the output parameters. By systematically perturbing inputs within defined ranges, the resulting effects on outputs allow the identification of key parameters among the model parameters shown in Figs. 1 and 3. The first-order Sobol index S_i quantifies the main effect of each input parameter x_i on the output y, independent of other input parameters, and is calculated in equation (3) as

$$S_i = \frac{V_i}{\mathrm{Var}(y)} = \frac{\mathrm{Var}_{x_i}\left(E_{x_{\sim i}}(y|x_i)\right)}{\mathrm{Var}(y)} \quad (3)$$

where $\mathrm{Var}(y)$ is the total variance of y, and $\mathrm{Var}_{x_i}(E_{x_{\sim i}}(y|x_i))$ is the variance of the expected output given x_i. $E_{x_{\sim i}}(y|x_i)$ represents the expectation of y over all inputs except x_i. The total-order index $S_{T,i}$ reflects the overall effect of each input, including both direct effects and interactions in equation (4):

$$S_{T,i} = 1 - \frac{\mathrm{Var}_{x_{\sim i}}\left(E_{x_{\sim i}}(y|x_{\sim i})\right)}{\mathrm{Var}(y)} = \frac{E_{x_{\sim i}}\left(\mathrm{Var}_{x_{\sim i}}(y|x_{\sim i})\right)}{\mathrm{Var}(y)} \quad (4)$$

Here, $S_{T,i}$ represents the cumulative effect of each parameter, including all higher-order interactions with other variables [53]. In this case, the conditional probability $E_{x_{\sim i}}(y|x_{\sim i})$ is calculated over the entire input space, excluding the i-th input parameter. Higher values of S indicate a greater influence of the corresponding input on the output. A perturbation of 25 % was applied to the initial values of the parameters and sampling was performed by Saltelli's extension of the Sobol' sequence. Since the results of a GSA are strongly dependent on the sample size, as clearly shown by Saxton et al. [54], a convergence analysis was performed, which can be found in the Appendix in Figure S-1. A sample size of $N = 2^{11}$ was chosen with converging means and statistical deviations of less than 5 % from the mean. The influence of all $D = 24$ cardiovascular system parameters was analyzed, resulting in $N(2D+2) = 102400$ model evaluations. The results are systolic pressure SP, diastolic pressure DP, mean arterial pressure MAP, mean pulmonary arterial pressure MPAP, pulmonary capillary wedge pressure PCWP, ECMO pump flow PF and cardiac output CO. Multiple GSA runs were performed using initial parameter values representative of patients in normo-, hypo- and hypertensive states with the ECMO pump speed set to 3440 rpm. These parameter values are listed in Table S-6. Additional analyses were performed for the normotensive condition at ECMO pump speeds of 2000, 2500, 4000 and 5000 rpm to ensure that the derived sensitivity indices were valid across the entire output space of the model in its present context of use. The average values of the predicted total

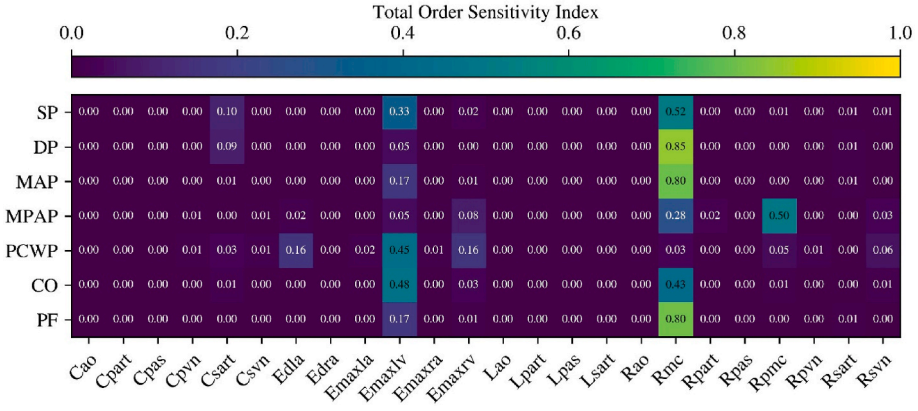

Fig. 3. Average total order sensitivity indices for a patient under normo-, hypo-, and hypertensive conditions. The ECMO pump speed was set to 3440 rpm for all three conditions, and additional sensitivity analyses were performed for normotension at 2000, 2500, 4000 and 5000 rpm.

order sensitivities for all described cases were used to identify the model parameters that account for 90 % of the sensitivity of each model output. The union of these parameters was selected as the final parameter subset.

2.4. Parameter identification

The selected parameters x were used to minimize the sum of the quadratic mean of the differences between the model predictions y_i and the patient data $\hat{y}_i$ described earlier, equation (5):

$$\text{Minimize } f(x) = \sum_{i=1}^{n} \left(\frac{y_i(x) - \hat{y}_i}{\hat{y}_i} \right)^2 \tag{5}$$

For this objective function, the parameter space was explored to verify that the function is smooth and differentiable within the relevant bounds. The results of this parameter space exploration can be found in Figure S-2 in the Appendix. A gradient-based optimization algorithm with bound constraints was used, and the gradients were calculated using AD. We used *SciPy's* least squares optimizer with trust region reflective algorithm as it is particularly efficient to exploit the least squares structure of the objective function. The bounds for each model parameter are shown in Table S-7 in the Appendix. Additionally, we used a multi-start approach based on the Tiktak algorithm developed in Arnoud et al. [55] with 70 runs of local optimizations. This was all implemented using the *Optimagic* package. This optimization approach combines exploration and exploitation to increase the likelihood of finding the global optimum. It repeatedly performs local optimizations starting from different initial parameter values until enough runs converge to the same solution. In the exploration phase, the algorithm evaluates the objective function at multiple initial parameter values that are randomly generated using Sobol sampling. In the exploitation phase, these parameter sets are sorted based on their objective function values. The first local optimization is performed from the best parameter set, while subsequent optimizations are initialized from a convex combination of the current best-known set and the next best sample point. To evaluate the performance of this optimization pipeline over a wide range of flows and pressures, we calibrated 30 distinct parameter sets from the 30 data points listed in Table 1. Thus, data points from each patient are treated independently.

2.5. Combined ECMO and CRRT study

For the analysis of the combined lung and kidney support therapy, the clinically relevant CRRT connection schemes shown in Fig. 2 were applied to a V-A ECMO circuit. From the previously fitted parameters, a 69-year-old female patient with cardiogenic shock and acute right heart failure was selected, who also received renal support during her therapy. A list of hemodynamic markers is given in Table S-8. A constant flow through the CRRT circuit of 0.2 L/min was set.

In a first step, the influence of the different connection types on the entire cardiac cycle was investigated for a constant pump speed of 3425 rpm. Next, the influence of the different connection types was examined at speeds between 1000 and 5000 rpm, which corresponds to the typical operating points of the Rotaflow RF-32 pump. In this second analysis, we compared only the mean of the clinical markers over the entire cardiac cycle. In addition, a GSA was again used to systematically investigate the influence of these two device-specific factors on the patient's hemodynamics. For this purpose, the model parameters were grouped into resistances $\mathbf{R}$ = {Rao, Rsart, Rmc, Rsvn, Rpas, Rpart, Rpmc, Rpvn}, compliances $\mathbf{C}$ = {Cao, Csart, Csvn, Cpas, Cpart, Cpvn}, inertances $\mathbf{L}$ = {Lao, Lsart, Lpas, Lpart}, and elastances $\mathbf{E}$ = {Edla, Edra, Emaxla, Emaxlv, Emaxra, Emaxrv}. These grouped factors were used together with the locations of drainage and return cannula as discrete values and the pump speed of the ECMO circuit as inputs to the GSA. This means that the individual effects of the parameters within each group cannot be separated but are considered as a combined single factor. This allows to quantify the total effect S_T of the entire group on the outputs [56,57]. The parameter bounds used to generate the samples are as described above. We added 25 % perturbation to the continuous input parameters and used sampling as previously described. In this way, the effects of small changes in the cardiovascular system parameters corresponding to clinical treatments of hypertension and hypotension (e.g. through inotropes or vasopressors) can be compared to changes in the extracorporeal system, such as ECMO pump speed and location of CRRT connection.

3. Results

3.1. Selection of most important model parameters for calibration

Fig. 3 shows the average total order sensitivity indices S_T for parameter values representative of a patient under different blood pressure conditions and ECMO pump speeds. This figure illustrates the effect of S_T of cardiovascular model parameters on all clinical measurements. The difference between total order and first or sensitivity indices can be seen in Figure S-5 in the Appendix. This can be used as a criterion for the linear dependence of the model parameters. Since all values are of the order of 10^{-3} or less, all parameters influence the model results in an independent manner. From Fig. 3 it can be seen that the systolic elastance of the left ventricle Emaxlv and the resistance of the systemic microcirculation Rmc have a significant influence on all outputs, as they account for 90 % of their total order sensitivity. The compliance of the systemic artery Csart mainly affects SP and DP. In contrast, the diastolic elastance of the left atrium Edla only affects

PCWP. Both the systolic elastance of the right ventricle Emaxrv and the resistance of the systemic vein Rsvn mainly affect MPAP and PCWP. In contrast, the resistance of the pulmonary microcirculation Rpmc shows a high value of S_T for MPAP. The distribution of model outputs resulting from the samples of the seven different GSA runs is shown in Figure S-3 in the Appendix. This illustrates that a wide range of clinically relevant scenarios of the model are covered.

Fig. 4 shows the sum of the total effect of each model parameter on all outputs across different patient blood pressure conditions and ECMO pump speeds. As before, Rmc and Emaxlv appear to have a significant global influence with values of 25.9 and 11.9. Parameters such as Rpmc, Emaxrv, Csart, Edla and Rsvn show a moderate cumulative effect with values of 4.0, 2.2, 1.8, 1.3 and 0.8. All parameters below the dashed vertical line are considered non-influential parameters and are not included in the model calibration process. The following seven parameters, displayed in orange, are selected for the parameter identification step: Rmc, Emaxlv, Rpmc, Emaxrv, Csart, Edla and Rsvn.

3.2. Model calibration

Fig. 5 shows Bland-Altman plots comparing the difference between simulated and measured data against their means for hemodynamic markers of flow and pressure. They include 30 data points from 8 V-A ECMO patients. The pressures (top) have a mean deviation of 0.28 mmHg and limits of agreement ranging from −7.5 to +8 mmHg. The flows (bottom) show a mean difference of −0.09 L/min and limits of agreement from −0.52 to +0.34 L/min. The data points are scattered around the mean difference line, with most falling within the limits of agreement, except for single data points of MAP and PF. A linear regression between the measured and the simulated data yields R^2 of 0.99 for the pressures and of 0.98 for the flows. Additional bar plots showing the error between the measured and predicted data are shown in Figure S-4.

3.3. Influence of CRRT connection scheme

This section examines the influence of different CRRT connection schemes on a single patient from the V-A ECMO cohort presented in Table 1. For this patient, the ECMO was operated at a constant pump speed of 3425 rpm, resulting in a flow of 3.7 L/min through the ECMO circuit. Fig. 6 a) shows the arterial, pulmonary arterial and venous pressures over two cardiac cycles. These are representative measures of the patient's systemic, pulmonary and venous circulatory systems and are used to derive most of the clinical markers listed in Table 1. The CRRT circuit affects the hemodynamics of the patient, with the greatest impact on the venous system, where a median pressure of 3.7 mmHg and a range (here always defined as max - min value) of 1.0 mmHg was observed across the different configurations simulated. In contrast, the smallest effect was seen on the arterial system, with a median pressure of 70.3 mmHg and a range of 5.4 mmHg. The patient's blood pressure is lowest when the access line is downstream of the ECMO pump (post pump) and the return line is upstream of the oxygenator (pre oxy, for configuration see Fig. 2 a)). To allow cross-referencing between all plots in Fig. 6, all results for this configuration are colored in blue. In contrast, blood pressures are highest for the access line placed pre pump and the return line placed post drainage cannula (post DC) (configuration Fig. 2 h)). The results for this configuration are colored orange.

Since V-A ECMO draws blood from the right atrium, it directly affects the amount of blood returning to the right ventricle (RV). To assess the impact of additional CRRT on the preload of the RV, Fig. 6 b) shows the RV pressure-volume (PV) loops for all connection schemes. When the access line is post pump and the return line is pre oxygenator (configuration Fig. 2 a)), this leads to a shift of the RV PV loops to lower pressures and volumes, as well as a reduction in stroke volume. For the combination pre pump – post DC, which results in the highest blood pressures in Fig. 6 a), a reverse effect can be observed (configuration Fig. 2 h)), giving a median end-systolic volume of 102.3 mL with a range of 24.5 mL and a median end-diastolic volume of 112.6 mL with a range of 27.7 mL. The median and range of the ventricular stroke volume and stroke work are 10.3 mL (with a range of 3.1 mL) and 10.1 mJ (with a range of 5.7 mJ), respectively.

The pressures in the access and return lines of the CRRT circuit are illustrated in Fig. 6 c) and 6 d). They are continuously monitored by the dialysis machine as they are important for safe and effective dialysis. Pressure alarms are triggered when certain limits are exceeded, indicating issues such as line occlusion or air in the system. Both pressure locations show high variability with a median of 161.4 and 258.2 mmHg, with a range of 296.6 and 295.9 mmHg for the access and return line, respectively. All pressures are below the maximum and above the minimum pressure alarms that are typically set as standard for CRRT devices. Furthermore, all pressures are positive, except for the connection where the access and return lines are upstream of the ECMO pump (configuration Fig. 2 h)).

Arterial, pulmonary arterial and venous pressures, as well as the pressure at the tip of the ECMO drainage cannula, are shown in Fig. 7 a) and b) for different CRRT connection types and ECMO flows. The latter is important in clinical practice to identify drainage insufficiency and minimize the risk of suction events. Varying the ECMO pump speed between 1000 and 5000 rpm results in ECMO flows of up to 6 L/min. With increasing ECMO flow, arterial pressures increase for all combinations, whereas pulmonary arterial and venous pressures decrease. The influence of CRRT connection types increases with increasing speed. At

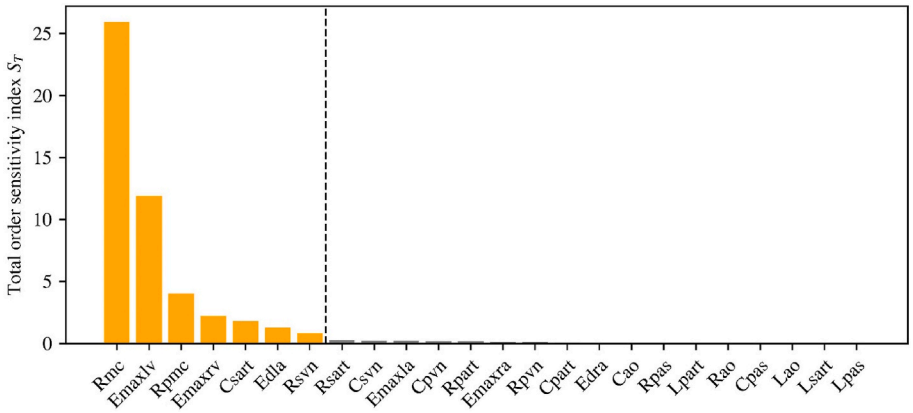

Fig. 4. Cumulative total order sensitivity indices of each model parameter derived from analyses across different patient blood pressure conditions and ECMO pump speeds. Parameters selected for model calibration are highlighted in orange. (For interpretation of the references to color in this figure legend, the reader is referred to the Web version of this article.)

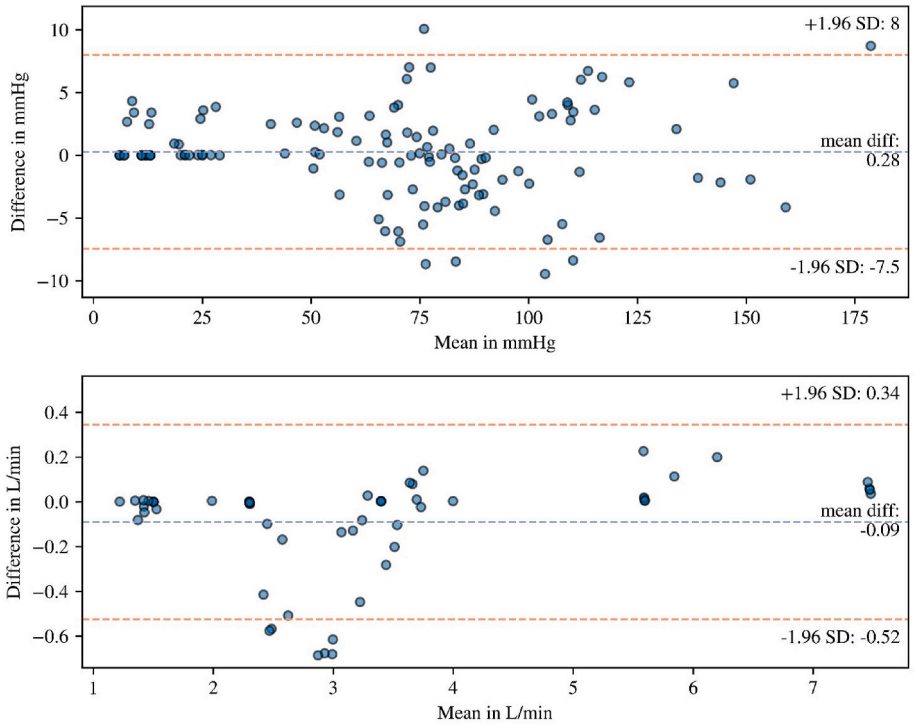

Fig. 5. Bland-Altman plot showing the mean of the simulated and the measured data versus their difference for hemodynamic markers of flow and pressure. A total of n = 30 data points from 8 V-A ECMO patients are included.

an ECMO flow of 1.2 L/min, arterial and ECMO drainage pressures have a median of 49.4 and 1.7 mmHg, respectively, and are within a range of 1.4 and 1.3 mmHg. However, at a much higher flow of 6 L/min, these values change to 85.2 and −129.6 mmHg with a range of 10.5 and 3.9 mmHg, respectively. At the maximum ECMO flow rates, the pulmonary artery pressure range for the various CRRT connection schemes simulated was found to be 5.3 mmHg. Except for the arterial blood pressure, the type of connection that yields the highest and lowest blood pressures is independent of the ECMO flow rate.

The pressures in the access and return lines of the CRRT circuit are shown in Fig. 7 c) and d). The same trend is seen as before. The mean pressures in the access and return lines of all combinations change significantly, from 2.6 to 136.5 mmHg with ranges of 81.3 and 81.6 mmHg at 1.2 L/min to 397.4 and 459.5 mmHg with ranges of 624.5 and 622.9 mmHg observed for the different connection schemes simulated at 6 L/min, respectively. When the access line is connected downstream of the ECMO pump and the return upstream of the oxygenator (configuration Fig. 2 a)), pressures increase with increasing ECMO flow. This behavior is observed for most combinations. The connection pre pump – post DC (Fig. 2 h)) shows the opposite behavior. This decrease in pressure with increasing ECMO flow is similar for all combinations with return lines upstream of the ECMO pump (Fig. 2 b), c), h), and i)). The maximum pressure alarms are reached at approximately 5 and 4 L/min for the access and return line, respectively. A minimum pressure alarm is only triggered for the return line at around 6 L/min.

The total order sensitivity indices S_T for the grouped cardiovascular parameters R, C, E and L, for the position of the CRRT circuit access and return lines, and for the ECMO pump speed for all model outputs are shown in Fig. 8. The ECMO speed (rpm) is the most sensitive parameter, and R has a particularly large influence on the patient's hemodynamics. The positions of the access and return lines are as sensitive to MPAP and CO as C, E, and L. Their combined contribution is highest for MPAP and CO, accounting for approximately 16 % of the total sensitivity. For systemic pressures and the pump flow, their influence is less than 10 %. This is further supported by the cumulative sensitivity indices shown in Figure S-6 in the Appendix. In summary, both locations of the access and return lines contribute to 90 % of the sensitivity of MPAP and CO. As can be seen in Figure S-7 in the Appendix, the GSA input samples resulted in a MAP between 50 and 100 mmHg and pump flows between 2 and 5 L/min, again representing normal, hypotensive and hypertensive states and the full range of ECMO operating conditions.

4. Discussion

The combination of ECMO and CRRT support represents a complex therapy, involving two extracorporeal circuits that interact with both each other and the patient's cardiovascular system. Currently, there are no guidelines for optimal connection schemes, and systematic analyses of how different CRRT connection schemes influence patient hemodynamics are lacking. In this study, we used a 0D computational model to investigate the mutual influence between the connection of CRRT, the degree of ECMO support, and the patient's circulation in the context of a single patient case study. Additionally, we conducted global sensitivity analyses and developed a parameter estimation pipeline tested on 30 data points from eight V-A ECMO patients. Our main findings are.

1. Model results suggest that CRRT can have a notable effect on the patient's cardiovascular system. This effect is highly dependent on the ECMO flow and leads to predicted changes in pulmonary artery pressure of up to 203 %.
2. GSA enables a systematic and agnostic approach to identifying key parameters that supports the parameter estimation process.
3. The established parameter estimation framework is robust in that it does not require any adjustment of the algorithm's parameters across different patient data.

An ECMO flow of 3.7 L/min in our in-silico study at a constant pump speed of 3425 rpm is comparable to the retrospective study by Wu et al. [21], which reported flows of 3.1 and 4.4 L/min. Also, the pressures at the access and return lines of the CRRT circuit are consistent with this study and the study by Wang et al. [20] and vary greatly depending on the connection location in the ECMO circuit, as also reported by Kashani

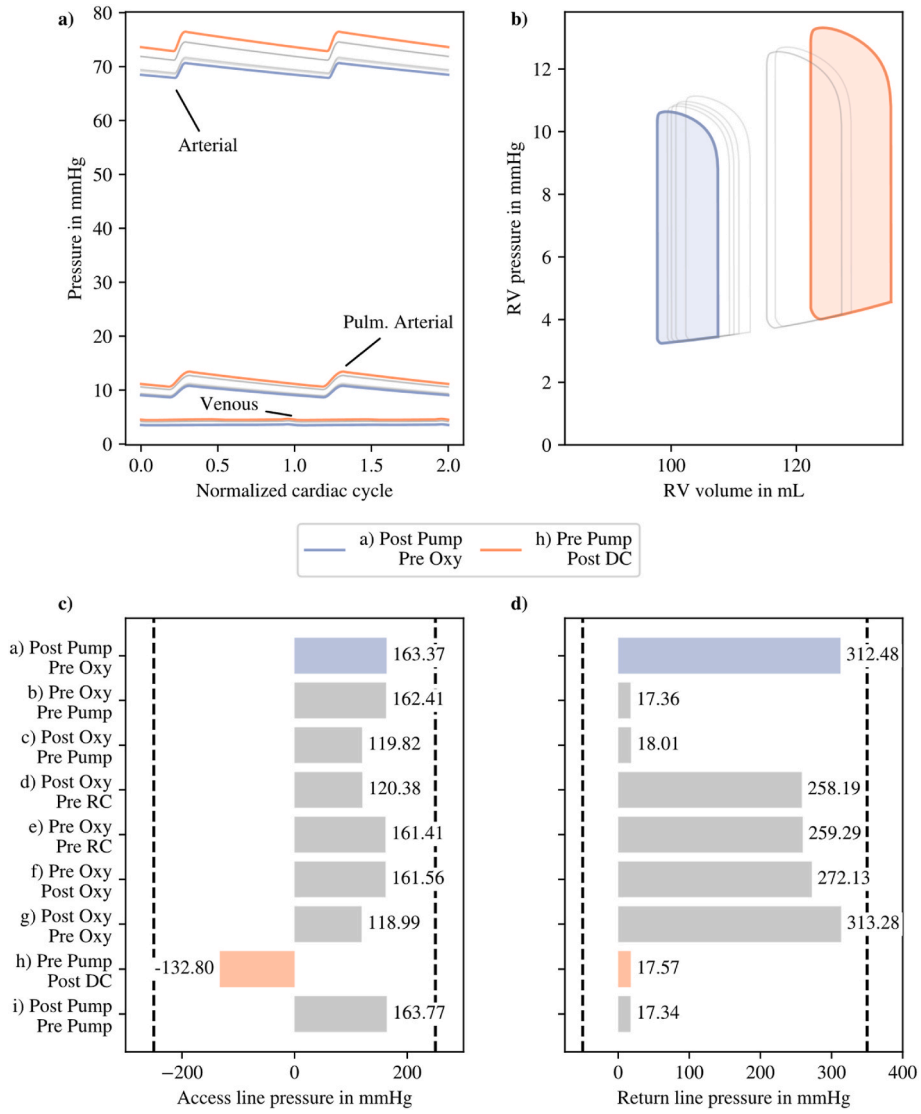

Fig. 6. Influence of different CRRT connections schemes on a) cardiovascular system, b) right ventricular (RV) PV loop and pressure of both access and return line of the CRRT circuit in c) and d), respectively. Combinations resulting in the highest and lowest arterial pressures are colored. The gray lines represent all other configurations. Coloring is applied to all subplots for cross-referencing purposes. See Fig. 2 for more details on the configurations. DC: drainage cannula, RC: return cannula. Common pressure alarms of CRRT circuit displayed in black dashed lines.

et al. [58]. Interestingly, while Wang et al. [20] observed negative pressures in the return line when connected upstream of the ECMO pump, both our results and those of Wu et al. [21] show positive return pressures for all configurations. This discrepancy could be due to the characteristics of the in-vitro setup used by Wang et al.

In method A from Wu et al., where the access line is connected downstream of the oxygenator and the return line upstream (our configuration Fig. 2 g)), the clinical data show a mean access line pressure of 175 mmHg (SD = 23 mmHg) and a mean return line pressure of 360 mmHg (SD = 8 mmHg). Our model predicts pressures of 119 and 313 mmHg, respectively. In method B, where the return line is changed to be upstream of the pump (our configuration Fig. 2 c)), the clinical data show a significantly lower mean return line pressure of 41 mmHg (SD = 13 mmHg) and an access line pressure of 171 mmHg (SD = 22 mmHg). Our model predicts 17 mmHg for the return line and 120 mmHg for the access line. These results suggest that our model can predict clinically realistic pressures in the CRRT circuit and is in line with the observed trends when the return line position is changed.

The in-vitro data from Wang et al. [20] show that both the pressures in the access and return lines and the influence of the CRRT connection increase with an increasing ECMO flow, with the pressure in the access line triggering the maximum alarm at around 5.5 L/min. This observation is also reflected in the predictions of our model. Sansom et al. [59] have found that high access line pressures correlate with early CRRT circuit failure and suggest that these pressures should be kept below 190 mmHg. Our model suggests that this can be maintained for ECMO flows up to 4.7 L/min when the access line is connected downstream the oxygenator and the return line is placed upstream the oxygenator (Fig. 2 g)), the ECMO return cannula (Fig. 2 d)), or the ECMO pump (Fig. 2 c)). In contrast, connecting the access line after the ECMO pump and the return line before the oxygenator (Fig. 2 a)) results in a pressure higher than 190 mmHg at an ECMO flow of 4 L/min already. This insight could help to extend circuit life without increasing the cost and complexity of the extracorporeal circuit by adding pressure sensors, as suggested in Na et al. [60].

Pressures in the entire ECMO circuit are consistent with the values reported by Sidebotham et al. [61]. Wu et al. [21] recommend connecting the CRRT circuit downstream to upstream of the oxygenator as depicted in Fig. 2 g). Looking at our in-silico results, this seems to be a good choice. Using our model, we can additionally confirm the advice to

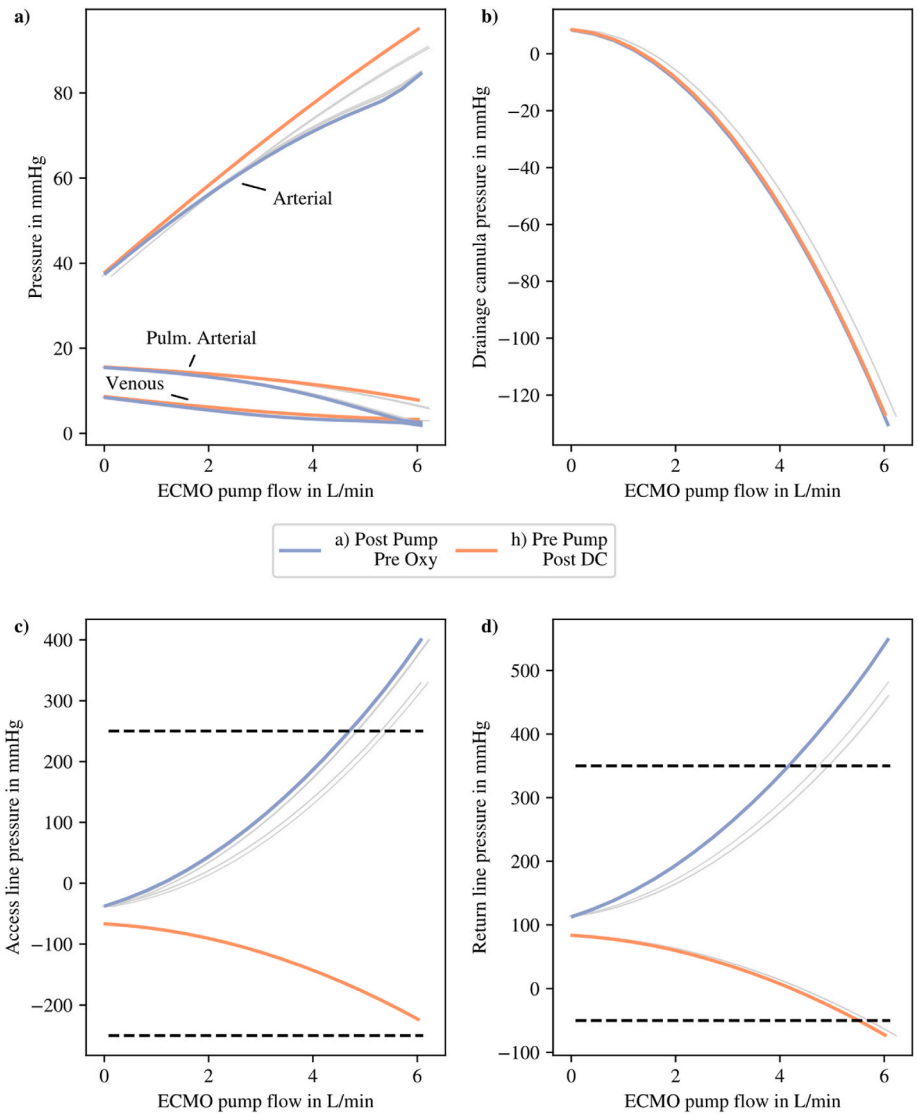

Fig. 7. Influence of different CRRT connections schemes with increasing ECMO pump flow on a) cardiovascular system, b) pressure in ECMO drainage cannula (DC) and both access and return line of the CRRT circuit in c) and d), respectively. Combinations resulting in the highest and lowest arterial pressures in the reference scenario presented in Fig. 6 are colored. The gray lines represent all other configurations. Coloring is applied to all subplots for cross-referencing purposes. See Fig. 2 for more details on the configurations. DC: drainage cannula, RC: return cannula. Common pressure alarms of CRRT circuit displayed in black dashed lines.

connect the return line upstream of the ECMO pump for high ECMO flows, as this reduces the pressure in the return line and the risk of triggering internal alarms of the CRRT device. Although many authors report a high risk of air leakage in this configuration due to negative pressures in the ECMO circuit upstream of the pump [7,11,12,19], Wu et al. did not observe this issue in their study. If the system setup does not allow the connection of the return line upstream of the ECMO pump, or if a pressure reduction is not critical, the connection upstream of the ECMO return cannula as depicted in Fig. 2 d) may provide a stable and safe alternative, as supported by the in-vivo data of Wang et al. [20]. This approach helps to manage high pressures and reduces the burden on nursing staff, as described by Kashani et al. [11] and de Tymowski et al. [19], potentially leading to fewer CRRT interruptions and maintaining normal operation even at high ECMO flows. This is particularly important in patients with high fluid overload.

The results of the total order sensitivity index S_T indicate that the position of both the access and return lines have an influence on the hemodynamics of the patient, which is particularly significant for MPAP and CO. For most model parameters, the first order sensitivity index S_1 for the different model parameters is negligibly small, indicating that their main effect is small. A closer look at the second order sensitivity indices S_2, which describe pairwise interactions, reveals strong interactions between access and return line locations and other parameters. The strongest interaction is between the resistances of the cardiovascular system R and the ECMO speed and between the locations of the access and return lines of the CRRT circuit. The value of S_2 also indicates that higher order interactions contribute to S_T. There could be several reasons for this. Firstly, higher ECMO flows increase the effect of different locations for the access and return lines of the CRRT circuit, as we have already seen in the results. In addition, the vascular resistance R may alter the flow dynamics so that blood is drawn and returned differently from the ECMO circuit. This would also suggest that the influence of the CRRT circuit and its possible combinations is different for each patient. In general, the significant interactions between CRRT access and return line locations with resistances of the cardiovascular system and ECMO speed demonstrate the complex interplay between the combined lung and kidney support therapy and the patient's cardiovascular system.

In summary, our computational model enabled a more systematic comparison of all possible CRRT connection schemes. It provided insight

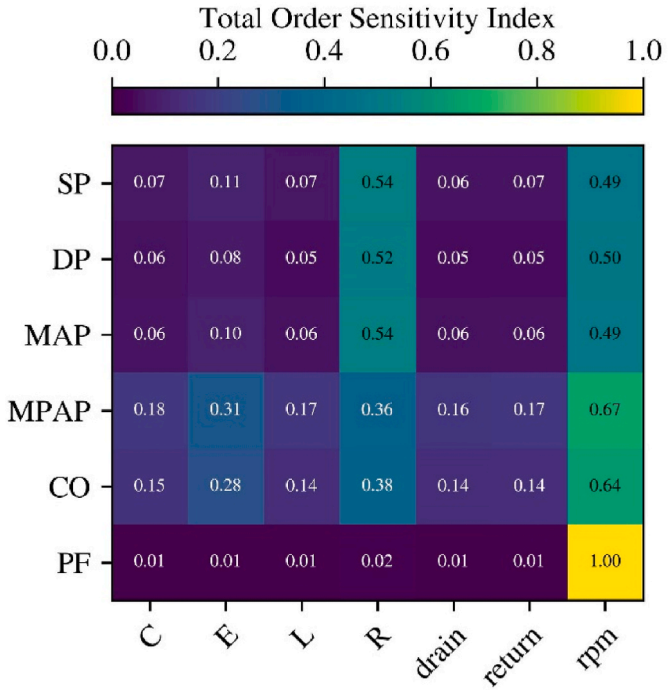

Fig. 8. Total order sensitivity indices for V-A ECMO patient from Global sensitivity analysis including CRRT connection scheme and ECMO pump speed. Grouping model parameters into resistances (R), compliances (C), and inertances (L) of the cardiovascular system and properties of the left and right atrium and ventricle (E).

into the effect of these schemes on measurements that are difficult or impossible to obtain in clinical practice and revealed greater variations in hemodynamic parameters, such as RV stroke volume and work, with increasing ECMO flow. The model predictions are consistent with measurements reported in the literature and highlight the complexity of ECMO and CRRT therapy. The model can provide hemodynamics on a patient-specific basis and can be adapted to routine clinical measurements through automated parameter fitting. The implementation of the GSA-based parameter estimation has been shown to be fast and effective, as demonstrated by testing it on multiple data points representing a broad range of ECMO therapy conditions.

This demonstrated that the model could be easily recalibrated without any further user input, such as adjusting algorithm parameters. This framework is open-source and promotes universal access to methods such as model sensitivity and parameter estimation, paving the way for digital twins that could be applied to various research questions, as promoted by Viceconti et al. [34]. However, further validation on clinical data is needed to quantify the predictive performance of the presented modeling pipeline.

The ODE system describing our model consists of 35 state equations with 90 parameters. Solving this model for 50 s on a single core of the Linux HPC CLAIX-2023 at RWTH Aachen University with an Intel Xeon 8468 Sapphire (2.1 GHz, 48 cores) took about 6.5 s. However, using just-in-time compilation with *JAX*, the runtime was reduced by a factor of 4.3 to about 1.5 s. For the parameter estimation procedure, using 35 cores on the same architecture, the average computation time for a single patient data point was 22 min. This performance is comparable to gradient-based calibration approaches such as those described by Salvador et al. [62], but significantly faster than other global strategies such as the Bayesian inference approach developed by Argus et al. [63].

The implemented parameter identification pipeline yields a parameter set that reproduces the clinical measurements. However, this solution is not unique and cannot be guaranteed to truly reflect the specific patient condition. The use of the Markov Chain Monte Carlo method, as proposed by Colunga et al. [48] and Argus et al. [63] is an approach for Bayesian parameter inference and could help to quantify the uncertainty of model predictions. Although our implementation allows for just-in-time compilation using *JAX*, which significantly reduces computation time, it may be necessary for such an approach to create a surrogate of the LPM to include uncertainty quantification in an efficient manner.

The GSA enables to determine the most influential model parameters and to consider the interactions between them. We demonstrated how to ensure the validity of the identified parameter subset by performing sensitivity analyses with different initial model parameters representative of different clinically relevant patient conditions. However, this does not determine whether the effects of the input parameters on a specific model output are very similar or the same. This is referred to as parameter orthogonality and is discussed in detail in Colunga et al. [37] and Saxton et al. [42]. In a next step, an orthogonality analysis will be added to the GSA to ensure complete identifiability of the input parameters used for personalization.

This computational model has the potential to support personalizing a combined lung and kidney support therapy to individual patient conditions. By applying the model to data from a larger ECMO cohort, more general conclusions could be drawn that may ultimately lead to standardized guidelines. In addition to optimizing the CRRT connection schemes, novel concepts such as the RenOx device, which integrates an oxygenator and a dialyzer in one system, would be of interest [64,65]. Such an approach would drastically reduce the complexity highlighted in this study.

5. Conclusion

In this study, we demonstrated that a GSA-informed parameter estimation process is computationally efficient and produces a high-quality fit to V-A ECMO patient data. The developed cardiovascular model can be used to model many different conditions of patients receiving V-A ECMO. The model suggests that the CRRT connection scheme can influence the hemodynamics of the patient and that the optimal choice may depend on the operating point and setup of the ECMO system. By integrating a discrete distribution for the locations of both the access and return lines of the CRRT circuit into the sample of a GSA, we were able to systematically quantify their influence and compare their significance to both the patient's cardiovascular properties and the ECMO pump flow.

In summary, the results of this study indicate that the direct effect of CRRT access and return line locations within the ECMO circuit alone is minimal, but their combined effect, when interacting with other parameters such as vascular resistance or ECMO pump speed, can be significant.

CRediT authorship contribution statement

Jan-Niklas Thiel: Writing – original draft, Visualization, Validation, Software, Methodology, Investigation, Formal analysis, Data curation, Conceptualization. **Ana Martins Costa:** Writing – review & editing. **Bettina Wiegmann:** Writing – review & editing, Resources, Project administration, Funding acquisition, Data curation. **Jutta Arens:** Writing – review & editing, Project administration, Funding acquisition. **Ulrich Steinseifer:** Writing – review & editing, Supervision, Resources, Project administration, Funding acquisition. **Michael Neidlin:** Writing – review & editing, Supervision, Project administration, Funding acquisition, Conceptualization.

Ethics statement

The study was approved by the Institutional Review Board of the Hannover Medical School and Aachen University Hospital. Only retrospectively acquired fully anonymized data was used.

Data availability

The model and code to perform the GSA and parameter identification can be found at the GitHub link https://github.com/nikithiel/ECLIPSE.

Funding

Funded by the Deutsche Forschungsgemeinschaft (DFG, German Research Foundation) SPP2014 "Towards the Artificial Lung" – project number: 447746988.

Declaration of competing interest

The authors declare that they have no known competing financial interests or personal relationships that could have appeared to influence the work reported in this paper.

Acknowledgements

This work was supported by the German Research Foundation (DFG) (project number 447746988, part of SPP 2014). Simulations were performed with computing resources granted by RWTH Aachen University under project rwth1463.

Appendix A. Supplementary data

Supplementary data to this article can be found online at https://doi.org/10.1016/j.compbiomed.2025.109668.

References

[1] T.V. Brogan, L. Lequier, R. Lorusso, G. MacLaren, G. Peek, Extracorporeal Life Support: the ELSO Red Book, fifth ed., 2017.
[2] H. Kim, J.H. Paek, J.H. Song, H. Lee, J.H. Jhee, S. Park, et al., Permissive fluid volume in adult patients undergoing extracorporeal membrane oxygenation treatment, Crit. Care 22 (2018) 270, https://doi.org/10.1186/s13054-018-2211-x.
[3] M. Schmidt, M. Bailey, J. Kelly, C. Hodgson, D.J. Cooper, C. Scheinkestel, et al., Impact of fluid balance on outcome of adult patients treated with extracorporeal membrane oxygenation, Intensive Care Med. 40 (2014) 1256–1266, https://doi.org/10.1007/s00134-014-3360-2.
[4] A.H. Smith, D.C. Hardison, C.R. Worden, G.M. Fleming, M.B. Taylor, Acute renal failure during extracorporeal support in the pediatric cardiac patient, Am. Soc. Artif. Intern. Organs J. 55 (2009) 412–416, https://doi.org/10.1097/MAT.0b013e31819ca3d0.
[5] C. Thongprayoon, W. Cheungpasitporn, P. Lertjitbanjong, N.R. Aeddula, T. Bathini, K. Watthanasuntorn, et al., Incidence and impact of acute kidney injury in patients receiving extracorporeal membrane oxygenation: a meta-analysis, J. Clin. Med. (2019), https://doi.org/10.3390/jcm8070981.
[6] B.C. Bridges, A. Dhar, K. Ramanathan, H.J. Steflik, M. Schmidt, K. Shekar, Extracorporeal life support organization guidelines for fluid overload, acute kidney injury, and electrolyte management, Am. Soc. Artif. Intern. Organs J. 68 (2022) 611–618, https://doi.org/10.1097/MAT.0000000000001702.
[7] H. Chen, R.-G. Yu, N.-N. Yin, J.-X. Zhou, Combination of extracorporeal membrane oxygenation and continuous renal replacement therapy in critically ill patients: a systematic review, Crit. Care 18 (2014) 675, https://doi.org/10.1186/s13054-014-0675-x.
[8] S.-S. Han, H.J. Kim, S.J. Lee, W.J. Kim, Y. Hong, H.-Y. Lee, et al., Effects of renal replacement therapy in patients receiving extracorporeal membrane oxygenation: a meta-analysis, Ann. Thorac. Surg. 100 (2015) 1485–1495, https://doi.org/10.1016/j.athoracsur.2015.06.018.
[9] S. Mitra, R.R. Ling, C.S. Tan, K. Shekar, G. MacLaren, K. Ramanathan, Concurrent use of renal replacement therapy during extracorporeal membrane oxygenation support: a systematic review and meta-analysis, J. Clin. Med. (2021), https://doi.org/10.3390/jcm10020241.
[10] L. Foti, G. Villa, S. Romagnoli, Z. Ricci, Acute kidney injury and extracorporeal membrane oxygenation: review on multiple organ support options, Int. J. Nephrol. Renovascular Dis. 14 (2021) 321–329, https://doi.org/10.2147/IJNRD.S292893.
[11] M. Ostermann, M. Connor, K. Kashani, Continuous renal replacement therapy during extracorporeal membrane oxygenation: why, when and how? Curr. Opin. Crit. Care 24 (2018) 493–503, https://doi.org/10.1097/MCC.0000000000000559.
[12] B. Seczyńska, W. Królikowski, I. Nowak, M. Jankowski, K. Szułdrzyński, W. Szczeklik, Continuous renal replacement therapy during extracorporeal membrane oxygenation in patients treated in medical intensive care unit: technical considerations, Ther. Apher. Dial. 18 (2014) 523–534, https://doi.org/10.1111/1744-9987.12188.
[13] Z. Ricci, S. Benelli, Fabio Barbarigo, Guilia Cocozza, N. Pettinelli, E. Di Luca, M. Mettifogo, et al., Nursing procedures during continuous renal replacement therapies: a national survey, Heart, Lung and Vessels (2015) 224–230.
[14] A.J. Tolwani, K.M. Wille, Anticoagulation for continuous renal replacement therapy, Semin. Dial. 22 (2009) 141–145, https://doi.org/10.1111/j.1525-139X.2008.00545.x.
[15] J.-J. Parienti, A.E. Dugué, C. Daurel, J.-P. Mira, B. Mégarbane, L.A. Mermel, et al., Continuous renal replacement therapy may increase the risk of catheter infection, Clin. J. Am. Soc. Nephrol. 5 (2010) 1489–1496, https://doi.org/10.2215/CJN.02130310.
[16] A. Oude Lansink-Hartgring, O. van Minnen, K.M. Vermeulen, W.M. van den Bergh, Hospital costs of extracorporeal membrane oxygenation in adults: a systematic review, Pharmacoecon Open 5 (2021) 613–623, https://doi.org/10.1007/s41669-021-00272-9.
[17] N. Srisawat, L. Lawsin, S. Uchino, R. Bellomo, J.A. Kellum, Cost of acute renal replacement therapy in the intensive care unit: results from the Beginning and Ending Supportive Therapy for the Kidney (BEST Kidney) study, Crit. Care 14 (2010) R46, https://doi.org/10.1186/cc8933.
[18] S. Costantini, M. Belliato, F. Ferrari, G. Gazzaniga, M. Ravasi, M. Manera, et al., A retrospective analysis of the hemolysis occurrence during extracorporeal membrane oxygenation in a single center, Perfusion 38 (2023) 609–621, https://doi.org/10.1177/02676591211073768.
[19] C de Tymowski, P. Augustin, H. Houissa, N. Allou, P. Montravers, A. Delzongle, et al., CRRT connected to ECMO: managing high pressures, Am. Soc. Artif. Intern. Organs J. 63 (2017) 48–52, https://doi.org/10.1097/MAT.0000000000000441.
[20] J. Wang, Q. Xu, J. Li, T. Wang, C. Zhong, Q. Chen, et al., Effect of different connection schemes of continuous renal replacement therapy and extracorporeal membrane oxygenation on arterial and venous pressure: an in vitro and in vivo study, Zhonghua Wei Zhong Bing Ji Jiu Yi Xue 34 (2022) 388–393, https://doi.org/10.3760/cma.j.cn121430-20210824-01261.
[21] J. Wu, X. Huang, Y. Mei, J. Lv, W. Li, D. Hu, et al., Impact of connecting methods of continuous renal replacement therapy device on patients underwent extracorporeal membrane oxygenation: a retrospectively observational study, Aust. Crit. Care 36 (2023) 695–701, https://doi.org/10.1016/j.aucc.2022.11.005.
[22] Y. Shi, Lawford Patricia, R. Hose, Review of Zero-D and 1-D Models of Blood Flow in the Cardiovascular System, 2011.
[23] T. Arts, T. Delhaas, P. Bovendeerd, X. Verbeek, F.W. Prinzen, Adaptation to mechanical load determines shape and properties of heart and circulation: the CircAdapt model, Am. J. Physiol. Heart Circ. Physiol. 288 (2005) H1943–H1954, https://doi.org/10.1152/ajpheart.00444.2004.
[24] T. Korakianitis, Y. Shi, Numerical simulation of cardiovascular dynamics with healthy and diseased heart valves, J. Biomech. 39 (2006) 1964–1982, https://doi.org/10.1016/j.jbiomech.2005.06.016.
[25] M. Broman, B. Frenckner, A. Bjällmark, M. Broomé, Recirculation during veno-venous extra-corporeal membrane oxygenation–a simulation study, Int. J. Artif. Organs 38 (2015) 23–30, https://doi.org/10.5301/ijao.5000373.
[26] M. Broomé, D.W. Donker, Individualized real-time clinical decision support to monitor cardiac loading during venoarterial ECMO, J. Transl. Med. 14 (2016) 4, https://doi.org/10.1186/s12967-015-0760-1.
[27] M. Broomé, Elira Maksuti, Anna Bjllmark, Bjrn Frenckner, Birgitta Janerot-Sjberg, Closed-loop Real-Time Simulation Model of Hemodynamics and Oxygen Transport in the Cardiovascular System, 2013.
[28] D.W. Donker, D. Brodie, J.P.S. Henriques, M. Broomé, Left ventricular unloading during veno-arterial ECMO: a simulation study, Am. Soc. Artif. Intern. Organs J. 65 (2019) 11–20, https://doi.org/10.1097/MAT.0000000000000755.
[29] D.W. Donker, M. Sallisalmi, M. Broomé, Right-left ventricular interaction in left-sided heart failure with and without venoarterial extracorporeal membrane oxygenation support-A simulation study, Am. Soc. Artif. Intern. Organs J. 67 (2021) 297–305, https://doi.org/10.1097/MAT.0000000000001242.
[30] C.J. Joyce, K. Shekar, D.A. Cook, A mathematical model of CO2, O2 and N2 exchange during venovenous extracorporeal membrane oxygenation, Intensive Care Med Exp 6 (2018) 25, https://doi.org/10.1186/s40635-018-0183-4.
[31] C.J. Joyce, K. Shekar, J. Walsham, Optimal settings at initiation of veno-venous extracorporeal membrane oxygenation: an exploratory in-silico study, Am. Soc. Artif. Intern. Organs J. 69 (2023) e28–e34, https://doi.org/10.1097/MAT.0000000000001849.
[32] S. Colasanti, V. Piemonte, E. Devolder, K. Zieliński, K. Vandendriessche, B. Meyns, L. Fresiello, Development of a computational simulator of the extracorporeal membrane oxygenation and its validation with in vitro measurements, Artif. Organs 45 (2021) 399–410, https://doi.org/10.1111/aor.13842.
[33] B de Lazzari, A. Iacovoni, K. Mottaghy, M. Capoccia, R. Badagliacca, C.D. Vizza, C de Lazzari, ECMO assistance during mechanical ventilation: effects induced on energetic and haemodynamic variables, Comput. Methods Progr. Biomed. 202 (2021) 106003, https://doi.org/10.1016/j.cmpb.2021.106003.
[34] M. Viceconti, M de Vos, S. Mellone, L. Geris, Position paper from the digital twins in healthcare to the Virtual Human Twin: a moon-shot project for digital health research, IEEE J Biomed Health Inform (2023), https://doi.org/10.1109/JBHI.2023.3323688.
[35] N.L. Bjørdalsbakke, J. Sturdy, E.M.L. Ingeström, L.R. Hellevik, Monitoring variability in parameter estimates for lumped parameter models of the systemic circulation using longitudinal hemodynamic measurements, Biomed. Eng. Online 22 (2023) 34, https://doi.org/10.1186/s12938-023-01086-y.
[36] N.L. Bjørdalsbakke, J.T. Sturdy, D.R. Hose, L.R. Hellevik, Parameter estimation for closed-loop lumped parameter models of the systemic circulation using synthetic data, Math. Biosci. 343 (2022) 108731, https://doi.org/10.1016/j.mbs.2021.108731.

[37] A.L. Colunga, M.J. Colebank, M.S. Olufsen, Parameter inference in a computational model of haemodynamics in pulmonary hypertension, J. R. Soc. Interface 20 (2023) 20220735, https://doi.org/10.1098/rsif.2022.0735.
[38] R. Laubscher, J. van der Merwe, P. Herbst, J. Liebenberg, Estimation of simulated left ventricle elastance using lumped parameter modelling and gradient-based optimization with forward-mode automatic differentiation based on synthetically generated noninvasive data, J. Biomech. Eng. (2023), https://doi.org/10.1115/1.4055565.
[39] R. Laubscher, J. van der Merwe, P.G. Herbst, J. Liebenberg, Estimation of pulmonary arterial pressure using simulated non-invasive measurements and gradient-based optimization techniques, MCA 27 (2022) 83, https://doi.org/10.3390/mca27050083.
[40] M. Salvador, F. Regazzoni, L. Dede, A. Quarteroni, Fast and Robust Parameter Estimation with Uncertainty Quantification for the Cardiac Function, 06.10, 2022.
[41] H. Saxton, T. Schenkel, I. Halliday, X. Xu, Personalised parameter estimation of the cardiovascular system: leveraging data assimilation and sensitivity analysis, Journal of Computational Science 74 (2023) 102158, https://doi.org/10.1016/j.jocs.2023.102158.
[42] H. Saxton, X. Xu, T. Schenkel, I. Halliday, Assessing input parameter hyperspace and parameter identifiability in a cardiovascular system model via sensitivity analysis, Journal of Computational Science 79 (2024) 102287, https://doi.org/10.1016/j.jocs.2024.102287.
[43] F. Huang, S. Ying, On-line parameter identification of the lumped arterial system model: a simulation study, PLoS One 15 (2020) e0236012, https://doi.org/10.1371/journal.pone.0236012.
[44] H. Huang, M. Yang, W. Zang, S. Wu, Y. Pang, In vitro identification of four-element windkessel models based on iterated unscented Kalman filter, IEEE Trans. Biomed. Eng. 58 (2011) 2672–2680, https://doi.org/10.1109/TBME.2011.2161477.
[45] R. Meiburg, W. Huberts, M.C.M. Rutten, F.N. van de Vosse, Uncertainty in model-based treatment decision support: applied to aortic valve stenosis, Int J Numer Method Biomed Eng 36 (2020) e3388, https://doi.org/10.1002/cnm.3388.
[46] S. Pant, C. Corsini, C. Baker, T.-Y. Hsia, G. Pennati, I.E. Vignon-Clementel, Data assimilation and modelling of patient-specific single-ventricle physiology with and without valve regurgitation, J. Biomech. 49 (2016) 2162–2173, https://doi.org/10.1016/j.jbiomech.2015.11.030.
[47] S. Pant, C. Corsini, C. Baker, T.-Y. Hsia, G. Pennati, I.E. Vignon-Clementel, Inverse problems in reduced order models of cardiovascular haemodynamics: aspects of data assimilation and heart rate variability, J. R. Soc. Interface (2017), https://doi.org/10.1098/rsif.2016.0513.
[48] A.L. Colunga, K.G. Kim, N.P. Woodall, T.F. Dardas, J.H. Gennari, M.S. Olufsen, B. E. Carlson, Deep phenotyping of cardiac function in heart transplant patients using cardiovascular system models, J. Physiol. 598 (2020) 3203–3222, https://doi.org/10.1113/JP279393.
[49] X. Zhang, D. Wu, F. Miao, H. Liu, Y. Li, Personalized hemodynamic modeling of the human cardiovascular system: a reduced-order computing model, IEEE Trans. Biomed. Eng. 67 (2020) 2754–2764, https://doi.org/10.1109/TBME.2020.2970244.
[50] M. Neidlin, C. Corsini, S.J. Sonntag, S. Schulte-Eistrup, T. Schmitz-Rode, U. Steinseifer, et al., Hemodynamic analysis of outflow grafting positions of a ventricular assist device using closed-loop multiscale CFD simulations: preliminary results, J. Biomech. 49 (2016) 2718–2725, https://doi.org/10.1016/j.jbiomech.2016.06.003.
[51] S. Boes, B. Thamsen, M. Haas, M.S. Daners, M. Meboldt, M. Granegger, Hydraulic characterization of implantable rotary blood pumps, IEEE Trans. Biomed. Eng. 66 (2019) 1618–1627, https://doi.org/10.1109/TBME.2018.2876840.
[52] I.M. Sobol, Global sensitivity indices for nonlinear mathematical models and their Monte Carlo estimates, Math. Comput. Simulat. (2001) 271–280.
[53] A. Puy, W. Becker, S. Lo Piano, A. Saltelli, A comprehensive comparison of total-order estimators for global, Int. J. Uncertain. Quantification 12 (2022) 1–18.
[54] Saxton H, Xu X, Schenkel T, Clayton RH, Halliday I. CONVERGENCE, sampling and total order estimator effects on parameter orthogonality IN GLOBAL SENSITIVITY ANALYSIS 2024. doi:10.1101/2024.02.25.582013.
[55] A. Arnoud, F. Guvenen, T. Kleineberg, Benchmarking Global Optimizers, National Bureau of Economic Research, 2019.
[56] T.A. Mara, S. Tarantola, Application of global sensitivity analysis of model output to building thermal simulations, Build. Simulat. 1 (2008) 290–302, https://doi.org/10.1007/s12273-008-8129-5.
[57] A. Saltelli, Global sensitivity analysis: the primer, Chichester England, Hoboken NJ: John Wiley (2008).
[58] K. Kashani, M. Ostermann, Optimizing renal replacement therapy for patients who need extracorporeal membrane oxygenation: cross-talk between two organ support machines, BMC Nephrol. 20 (2019) 404, https://doi.org/10.1186/s12882-019-1602-9.
[59] B. Sansom, B. Riley, A. Udy, S. Sriram, J. Presneill, R. Bellomo, Continuous renal replacement therapy during extracorporeal membrane oxygenation: circuit haemodynamics and circuit failure, Blood Purif. 52 (2023) 522–531, https://doi.org/10.1159/000529928.
[60] S.J. Na, H.J. Choi, C.R. Chung, Y.H. Cho, H.R. Jang, G.Y. Suh, K. Jeon, Using additional pressure control lines when connecting a continuous renal replacement therapy device to an extracorporeal membrane oxygenation circuit, BMC Nephrol. 19 (2018) 369, https://doi.org/10.1186/s12882-018-1172-2.
[61] D. Sidebotham, S.J. Allen, A. McGeorge, N. Ibbott, T. Willcox, Venovenous extracorporeal membrane oxygenation in adults: practical aspects of circuits, cannulae, and procedures, J. Cardiothorac. Vasc. Anesth. 26 (2012) 893–909, https://doi.org/10.1053/j.jvca.2012.02.001.
[62] M. Salvador, F. Regazzoni, L. Dede, A. Quarteroni, Fast and robust parameter estimation with uncertainty quantification for the cardiac function, Comput. Methods Progr. Biomed. 231 (2023) 107402, https://doi.org/10.1016/j.cmpb.2023.107402.
[63] F. Argus, D. Zhao, T.P. Babarenda Gamage, M.P. Nash, G.D. Maso Talou, Automated model calibration with parallel MCMC: applications for a cardiovascular system model, Front. Physiol. 13 (2022) 1018134, https://doi.org/10.3389/fphys.2022.1018134.
[64] A. Martins Costa, F.R. Halfwerk, J.-N. Thiel, B. Wiegmann, M. Neidlin, J. Arens, Effect of hollow fiber configuration and replacement on the gas exchange performance of artificial membrane lungs, J. Membr. Sci. 680 (2023) 121742, https://doi.org/10.1016/j.memsci.2023.121742.
[65] A. Martins Costa, F.R. Halfwerk, J.-N. Thiel, B. Wiegmann, M. Neidlin, J. Arens, Influence of utilizing hemodialysis membranes outside-in on solute clearance and filtration efficiency – one step towards a novel combined lung and kidney support device, J. Membr. Sci. 698 (2024) 122575, https://doi.org/10.1016/j.memsci.2024.122575.